

# Stereotomography assisted by migration of attributes

Sylvain Nguyen<sup>1,†</sup>, Reda Baina<sup>2</sup>, Mathias Alerini<sup>1,‡</sup>, Gilles Lambaré<sup>1,\*,§</sup>,  
Vincent Devaux<sup>3</sup> and Mark Noble<sup>1</sup>

<sup>1</sup>École des Mines de Paris, Centre de Recherche en Géophysique, 35, rue Saint Honoré, 77305 Fontainebleau, France, <sup>2</sup>Opera, Pau University, Batiment IFR, Rue Jules Ferry, 64000 Pau, France, and <sup>3</sup>Total, CSTJF, rue Larribau, 64018 Pau, France

Received July 2007, revision accepted December 2007

## ABSTRACT

Depth velocity model building remains a difficult step within the seismic depth imaging sequence. Stereotomography provides an efficient solution to this problem but was limited until now to a picking of seismic data in the prestack time un-migrated domain. We propose here a method for stereotomographic data picking in the depth migrated domain. Picking in the depth migrated domain exhibits the advantage of a better signal-to-noise ratio and of a more regular distribution of picked events in the model, leading to a better constrained tomographic inverse problem. Moreover, any improvement on the velocity model will improve the migrated results, again leading to improved picking. Our strategy for obtaining a stereotomographic dataset from a prestack depth migration is based on migration of attributes (and not on a kinematic demigration approach!). For any locally coherent event in the migrated image, migration of attributes allows one to compute ray parameter attributes corresponding to the specular reflection angle and dip. For application to stereotomography, the necessary attributes are the source/receiver locations, the traveltimes and the data slopes. For the data slope, when the migration velocity model is erroneous, some additional corrections have to be applied to the result of migration of the attributes. Applying these corrections, our picking method is theoretically valid whatever the quality of the migration velocity model. We first present the theoretical aspects of the method and then validate it on 2D synthetic and real seismic reflection data sets.

## INTRODUCTION

Velocity model building still remains a serious bottleneck for reflection seismic depth imaging. Several questions remain open for this challenge, as the need for picking, the domain for the picking, the choice of the cost function, the use of smooth or blocky models . . . This last point is still a debated issue, trying to accommodate various points of view and case studies. Here we use a smooth representation of the velocity field, allowing us to compute continuous geometrical spread-

ing and paraxial ray quantities (e.g., Wang and Houseman 1995) and appropriate for ray based preserved amplitude migration (Thierry *et al.* 1999).

For velocity model building, up to now only local optimization methods have been used successfully for real sized applications. Most frequently, they work in the depth migrated domain and address the flattening of the common-image gathers. Both with (Al-Yahya 1989) and without-picking methods (Symes 1998; Chauris and Noble 2001) have been investigated. In industry, picking-based approaches are still the most frequently used, since they enable easier and faster minimization of the cost function and allow one to compensate for imperfect preprocessing. However, the picking remains a critical point in all these processing sequences and it is precisely this point that we address in the present paper.

\*E-mail: gilles.lambare@free.fr

†Now at: Beicip Franlab, 232, avenue Napoléon-Bonaparte BP 213, 92502 Rueil-Malmaison Cedex, France.

‡Now at: Sintef Petroleum Research, No-7465, Trondheim, Norway.

§Now at: CGGVeritas, 1 rue Léon Migaux, 91341 Massy Cedex, France.

Numerous picking-based methods have been proposed for computing depth velocity models from seismic reflection data. It remains one of the most difficult tasks in the depth velocity model building workflow. Stereotomography (Billette and Lambaré 1998; Billette *et al.* 2003) was developed to remedy the difficult interpretative picking required by horizon-based tomographic approaches (Farra and Madariaga 1988). Stereotomography belongs to the family of slope tomographic methods (Riabinkin 1957; Sword 1986). The idea is to use kinematic information from locally coherent events described by their central source and receiver position, their central time and their local slopes in the prestack dataset. Stereotomography appears as a generalization of formerly existing slope tomographic methods, with the benefits of robustness and efficiency. The method has been extended to 3D (Chalard *et al.* 2000; Chalard and Lambaré 2005), to converted waves (Alerini *et al.* 2002, 2007), to borehole data (Gosselet, Le Bégat and Petersen 2005) and has finally resulted into a robust and efficient semi-automated approach for estimating depth velocity models (Lambaré *et al.* 2004).

In all these studies, stereotomographic picking was done in the prestack un-migrated domain. This choice has demonstrated its efficiency but picking in some other, more appropriate, domain may offer serious advantages. For example, Lavaud, Baina and Landa (2004) and Neckludov, Baina and Landa (2005) demonstrated the benefit of stereotomographic picking from common-reflection stack images and common-reflection stack attributes (Jäger *et al.* 2001) with a better signal-to-noise ratio and easier interpretation. The prestack depth migrated domain also has many advantages as a more controlled coverage of the velocity model, allowing better constraint of the optimization. This explains why picking in the migrated domain is still the most frequently used, and various workflows involving migration, picking and demigration have been proposed (Apostoiu-Marin and Ehinger 1997; Le Stunff and Grenier 1998; Wang, White and Pratt 2000). Concerning the use of locally coherent events picked in the depth migrated domain, the contribution by Chauris *et al.* (2002a,b) was an important breakthrough. It demonstrated that there was a direct connection between locally coherent events in the depth-migrated domain and in the un-migrated time domain. The connection between both involves kinematic migration or demigration processes and allows for a stereotomographic picking in the depth-migrated domain. In the present paper we directly rely on this work. We propose a depth domain picking for stereotomography based on migration of tomographic attributes. Compared to the Chauris *et al.* (2002a,b)'s work, our choice is to perform a single-pass migration and picking

(with the benefit of efficiency) and to replace the kinematic demigration by the migration of attributes process proposed by Bleistein (1987) with the benefit of consistency between migration and demigration.

Initially, the migration of the attributes was proposed for obtaining specular reflection angle. Two Kirchhoff type migrations are performed with the same data and velocity model but with a different amplitude in the migration kernel (the data set must be a single channel data set – common offset – common shot – common receiver). For example, multiplying the migration kernel by the reflection angle (as a seismic attribute), the local ratio of the two migrated images gives the specular reflection angle all over the considered target. It is often used in amplitude versus offset (or angle) analysis (Baina, Thierry and Calandra 2002). In a similar way, it can be used for attributes required for tomography, as for example, the source/receiver locations, the two-way times and the associated slopes (Chen 2000). Note that the extracted specular values are the ones relevant for the depth migration process whatever the quality of the migration velocity model. When the velocity model is erroneous, some appropriate corrections may be required to obtain the corresponding attributes in the prestack time un-migrated domain. This is the case for the slopes of the events in the un-migrated domain, for which Chauris *et al.* (2002a) and Nguyen *et al.* (2002b) derived the associated corrections.

Stereotomography has already been presented in numerous papers. In the present paper, we focus on the presentation of the new stereotomographic picking in the depth-migrated domain. The approach is tested with a synthetic example and compared to a 'classical' stereotomographic picking in time. Finally, we present an application on real data of the full depth velocity model building sequence, with a comparison between the time and depth picking approaches.

## THEORETICAL ASPECTS

### Migration of attributes: theory

Let us consider a common-offset Kirchhoff depth migration. The migrated image,  $\mathcal{I}(\mathbf{x}, h_0)$ , obtained at location,  $\mathbf{x}$ , for offset  $h_0$ , can be expressed as an integral over the midpoint location,  $\sigma$ ,

$$\mathcal{I}(\mathbf{x}, h_0) = \int d\sigma \mathcal{A}(\sigma, \mathbf{x}, h_0) \mathcal{D}(\sigma, T^{ray}(\sigma, \mathbf{x}, h_0), h_0) \quad (1)$$

where  $\mathcal{A}(\sigma, \mathbf{x}, h_0)$  denotes the amplitude of the kernel of the migration operator,  $\mathcal{D}(\sigma, t, h_0)$  denotes the preprocessed traces recorded at midpoint location,  $\sigma$ , at time,  $t$  and at offset,  $h_0$ , and  $T^{ray}(\sigma, \mathbf{x}, h_0)$  denotes two-way traveltime function used in the kernel of the migration operator. This migration formula

can be also given in the time frequency domain

$$\mathcal{I}(\mathbf{x}, h_0) = \int d\omega \int d\sigma \mathcal{A}(\sigma, \mathbf{x}, h_0) \mathcal{D}(\sigma, \omega, h_0) e^{-i\omega T^{ray}(\sigma, \mathbf{x}, h_0)}, \quad (2)$$

where  $\omega$  is then the angular frequency. Our convention for direct and inverse Fourier transform is  $f(\omega) = \int_{-\infty}^{+\infty} dt f(t) e^{i\omega t}$  and  $f(t) = \frac{1}{2\pi} \int_{-\infty}^{+\infty} d\omega f(\omega) e^{-i\omega t}$ .

Let us now assume that the un-migrated data volume consists of a superposition of coherent events and let us consider one of these events. It can be described by

$$\mathcal{D}(\sigma, \omega, h_0) = S(\sigma, h_0, \omega) e^{i\omega T^{data}(\sigma, h_0)}, \quad (3)$$

where  $S(\sigma, h_0, \omega)$  denotes the wavelet in the frequency domain, and  $T^{data}(\sigma, h_0)$  denotes the time curve of the event. If we assume that locally the event has very gentle lateral variations of its wavelet (which is the definition of a locally coherent event), we can write

$$S(\sigma, h_0, \omega) \approx A(\sigma, h_0) S(\omega), \quad (4)$$

where we have restricted wavelet variations to amplitude variations,  $A(\sigma, h_0)$ , while the normalized wavelet is fixed to  $S(\omega)$ .

Introducing relations (3) and (4) into relation (2), we get the common offset migrated image of an event. It is indeed an integral over  $\sigma$ , which vanishes when  $\omega$  goes to  $\infty$ , except in the vicinity of stationary points  $\sigma_c$ . Such points are defined by the stationary phase theorem (Bleistein and Handelsman 1975; Bender and Orszag 1978), which imposes:

$$\frac{\partial [T^{data}(\sigma_c, h_0) - T^{ray}(\sigma_c, \mathbf{x}, h_0)]}{\partial \sigma} = 0$$

$$\frac{\partial T^{data}(\sigma_c, h_0)}{\partial \sigma} = \frac{\partial T^{ray}(\sigma_c, \mathbf{x}, h_0)}{\partial \sigma}. \quad (5)$$

Relation (5) means that the slope of the two-way traveltime function used in the kernel of the migration operator has to fit with the slope of the locally coherent event (see Fig. 1). Indeed, a locally coherent event in a common offset gather of traces will focus in depth at the position,  $\mathbf{x}$ , if the traveltime function  $T^{ray}(\sigma, \mathbf{x})$  becomes tangent to the time curve of the event,  $T^{data}(\sigma)$ , for variations of  $\sigma$ . For a given event, offset,  $h_0$  and migrated position  $\mathbf{x}$ , when it exists, we call  $\sigma_c$ , the stationary point for the migration (we also speak of a specular point).

Asymptotically, the contribution of the vicinity of a specular point can be given by the stationary phase approximation (Bleistein and Handelsman 1975; Bender and Orszag 1978). Within this approximation, it reduces to:

$$\mathcal{I}(\mathbf{x}, h_0) \approx \mathcal{A}(\sigma_c, \mathbf{x}, h_0) \int d\omega \frac{\mathcal{D}(\sigma_c, \omega, h_0)}{\sqrt{2\pi i \omega \frac{\partial^2 \Delta T(\sigma_c, \mathbf{x}, h_0)}{\partial \sigma^2}}} = e^{i\omega T^{ray}(\sigma_c, \mathbf{x}, h_0)}, \quad (6)$$

where  $\Delta T(\sigma_c, \mathbf{x}, h_0) = T^{data}(\sigma_c, h_0) - T^{ray}(\sigma_c, \mathbf{x}, h_0)$ .

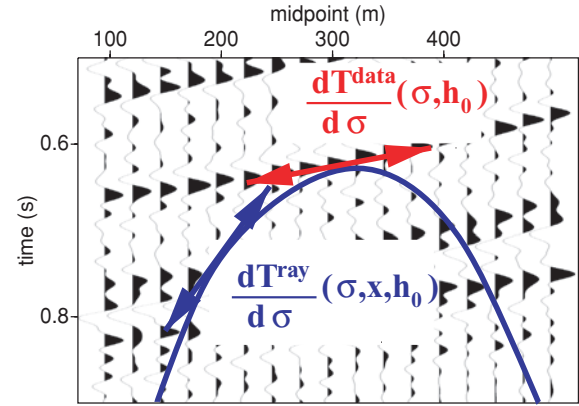


**Figure 1** Imaging condition. An event in a common offset gather will migrate at position  $\mathbf{x}$  if the observed time,  $T^{ray}$  and the migration traveltime,  $T^{data}$  match and if the slope of the migration travel time ( $\partial T^{ray}/\partial \sigma(\sigma, \mathbf{x}, h_0)$  for  $\mathbf{x}$  fixed) matches with the slope of the observed traveltime curve,  $\partial T^{data}/\partial \sigma(\sigma, h_0)$ .

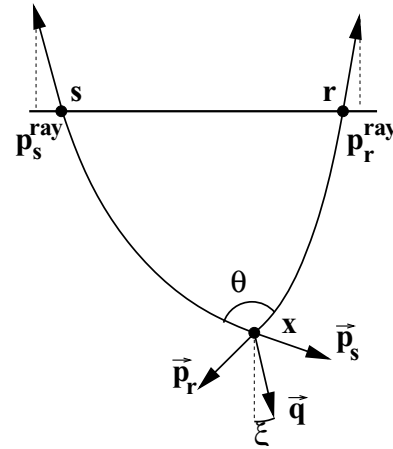


**Figure 2** The ray parameters involved in the stereotomographic attributes migration. The vector  $\mathbf{q}$  is the sum of the slowness vectors,  $\mathbf{p}_s$  and  $\mathbf{p}_r$ , of shot and receiver ray segments at the image point  $\mathbf{x} = (x, z)$ .  $\xi$  is the local geological dip and  $\theta$  is the aperture angle.  $p_s^{ray}$  and  $p_r^{ray}$  are the horizontal components of upwards slowness vectors at the acquisition surface.

From this expression we see that, when we introduce a weight,  $\mathcal{K}(\sigma, \mathbf{x}, h_0)$ , in the migration kernel (2),

$$\mathcal{I}_{\mathcal{K}}(\mathbf{x}, h_0) = \iint d\omega d\sigma \mathcal{K}(\sigma, \mathbf{x}, h_0) \mathcal{A}(\sigma, \mathbf{x}, h_0) \mathcal{D}(\sigma, \omega, h_0) e^{-i\omega T^{ray}(\sigma, \mathbf{x}, h_0)}, \quad (7)$$

we obtain a depth migrated image multiplied locally by the value of the weight for the local specular contribution,

$$\mathcal{I}_{\mathcal{K}}(\mathbf{x}, h_0) \approx \mathcal{K}(\sigma_c, \mathbf{x}, h_0) \mathcal{I}(\mathbf{x}, h_0). \quad (8)$$

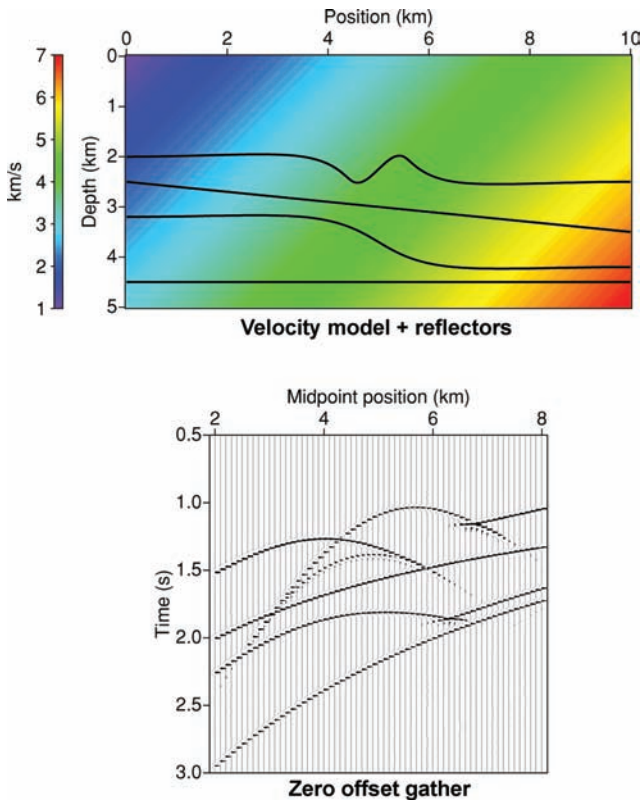


Figure 3 2D synthetic case. Top: velocity model with the location of the four reflectors. Bottom: common-offset gather for offset = 100 m.

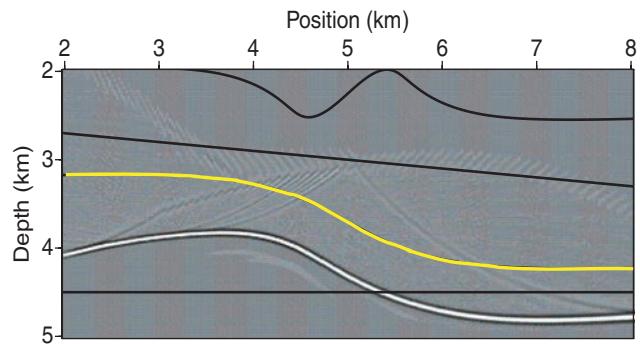


Figure 4 2D synthetic case. Common offset depth migrated panel used for the test (offset = 100 m). An erroneous velocity model was used for the migration. The true reflector position is superimposed in yellow. Migration artefacts (aliasing, truncation effects, ...) appear due to the high gain value used for the display.

The use of this property was proposed by Bleistein (1987) for estimating in a double-migration process, specular quantities associated to a depth migrated image (We also call this process migration of attributes). The weighting factor  $\mathcal{K}(\sigma, \mathbf{x}, h_0)$  may be any ray based attribute, i.e., reflection angle, incidence angle, source or receiver locations, one-way or two-way travel

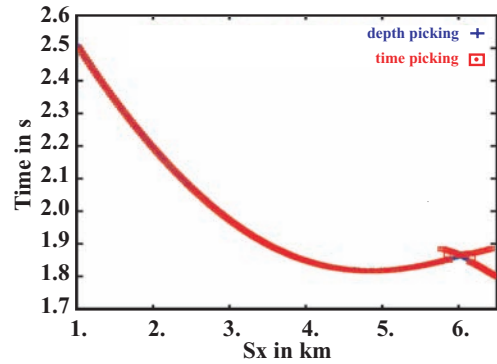


Figure 5 2D synthetic case. Comparison of the two-way traveltime curve versus shot position  $s_x$  obtained by picking in the time domain (red squares) with one picking in the time domain (red squares) with one obtained picking in the depth domain with migration of attributes (blue crosses).

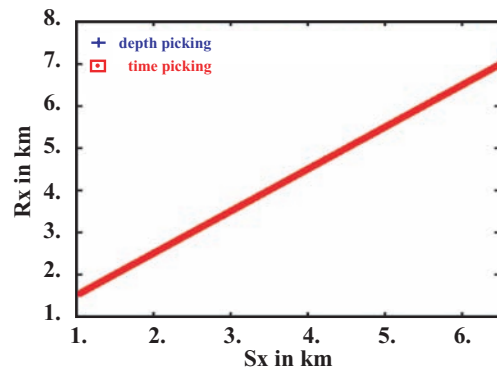
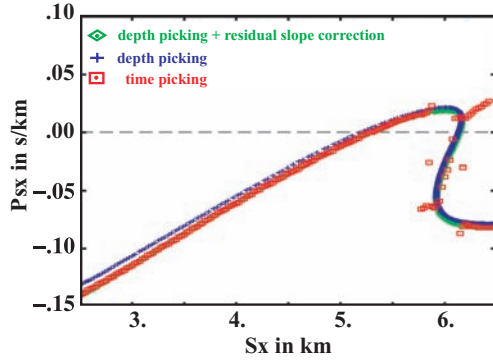


Figure 6 2D synthetic case. Comparison of the receiver position  $r_x$  curve versus shot position  $s_x$  obtained by picking in the time domain (red squares) with the one obtained picking in the depth domain with migration of attributes (blue crosses).

times ... To obtain one of these specular attributes we have to compute a second migrated image  $\mathcal{I}_{\mathcal{K}}(\mathbf{x}, h_0)$ . In practice, the two migrations are performed during the same migration loop in order to save computing time and the attribute map is obtained for a given offset via the ratio of the two common offset migrated images (Bleistein 1987; Hubral, Schleicher and Tygel 1996; Tygel, Schleicher and Hubral 1996):

$$\mathcal{K}(\sigma_c, \mathbf{x}, h_0) = \frac{\mathcal{I}_{\mathcal{K}}(\mathbf{x}, h_0)}{\mathcal{I}(\mathbf{x}, h_0)}. \tag{9}$$

Note that the approach is only valid for image points,  $\mathbf{x}$ , for which a single stationary point exists and that some smoothing and regularization has to be introduced to insure the robustness of the process (Baina *et al.* 2002). Note also that this approach can also be developed for common angle or common shot migrated gathers as shown by Chauris *et al.* (2001) or Chauris (2000).



**Figure 7** 2D synthetic case. Comparison of the receiver position  $p_{sx}$  curve versus shot position  $s_x$  obtained by picking in the time domain (red squares) with the one obtained picking in the depth domain after migration of attributes before (blue crosses) and after residual slope correction (green diamonds).

### Migration of stereotomographic attributes

In the present study, we plan to use migration of attributes to obtain stereotomographic attributes. These attributes involve the local slopes of locally coherent events in common-shot and common-receiver gathers  $p_s^{data}$  and  $p_r^{data}$ , in addition to the classical tomographic parameters, source and receiver positions,  $(s, r)^{data}$ , and traveltime curve,  $T^{data}$  (Billette and Lambaré 1998). For a given set of  $N$  local events in a depth migrated image, the purpose is to obtain the associated stereotomographic dataset,

$$\mathbf{d} = [(s^{data}, r^{data}, T^{data}, p_s^{data}, p_r^{data})_n]_{n=1}^N. \quad (10)$$

As we have seen, the migration of attributes provides specular attributes associated with depth migration. The idea is to use these attributes to derive local characteristics of the

events. There are definitely some links between locally coherent events picked either in the time or in the depth domain for a given velocity model (Liu 1997; Chauris *et al.* 2002a). They are described by the common offset imaging equations,

$$T^{data}(s, r) = T^{ray}(s, r, \mathbf{x}), \quad (11)$$

$$(p_s^{data} - p_s^{ray}) + (p_r^{data} - p_r^{ray}) = 0, \quad (12)$$

$$(p_s^{data} - p_s^{ray}) - (p_r^{data} - p_r^{ray}) = q_z^{ray} \tan(\varphi), \quad (13)$$

where  $\varphi$  is the residual slope of the depth migrated event in the common-image gather,  $\tan(\varphi) = \frac{\partial Z^{mig}}{\partial b}(Z^{mig}(\mathbf{x}, b))$  is the depth migration curve of event  $T^{data}(\mathbf{x}, b)$ . Let  $\mathbf{q}$  be the sum of the two slowness vectors at point  $\mathbf{x}$  (Fig. 2),

$$\mathbf{q} = \frac{\partial T^{ray}}{\partial \mathbf{x}} = \mathbf{p}_s(\mathbf{x}) + \mathbf{p}_r(\mathbf{x}). \quad (14)$$

We have:  $|\mathbf{q}| = 2u(\mathbf{x}) \cos(\theta)$ ,  $u(\mathbf{x})$  being the slowness (inverse of the velocity), and  $\theta(s, \mathbf{x}, r)$  being the aperture angle. The projection of  $\mathbf{q}$  on the vertical axis gives the stretching factor (Tygel, Schleicher and Hubral 1994):

$$q_z^{ray} = 2u(\mathbf{x}) \cos(\theta) \cos(\xi) \quad (15)$$

where  $\xi(s, \mathbf{x}, r)$  denotes the angle associated to the dip (Fig. 2).

Considering equations (11), (12) and (13), we see that source and receiver positions,  $(s^{data}, r^{data})$  and observed time,  $T^{data}$ , can be directly obtained by migration of attributes using weights,  $s, r$  and  $T^{ray}$ , respectively. For the slopes  $(p_s^{data}, p_r^{data})$  we see that in addition to the need for a migration of attributes of  $(p_s^{ray}, p_r^{ray})$ , we need to apply a correction involving the stretching factor,  $q_z^{ray}$ , and the residual slope of the depth migrated event in the common-image gather,  $\varphi$  (equation 13).

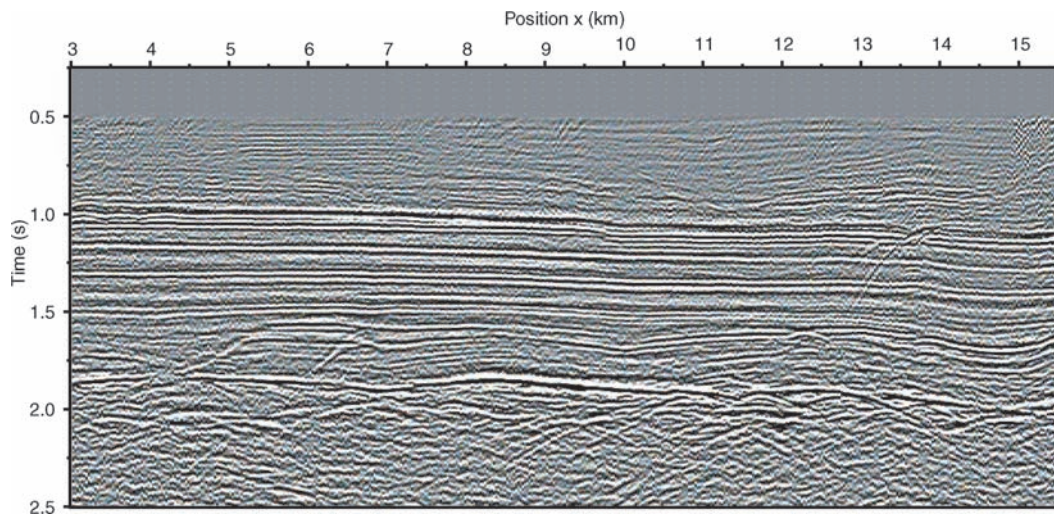


**Figure 8** Real data case. Common offset gather of the data set (offset = 500 m).

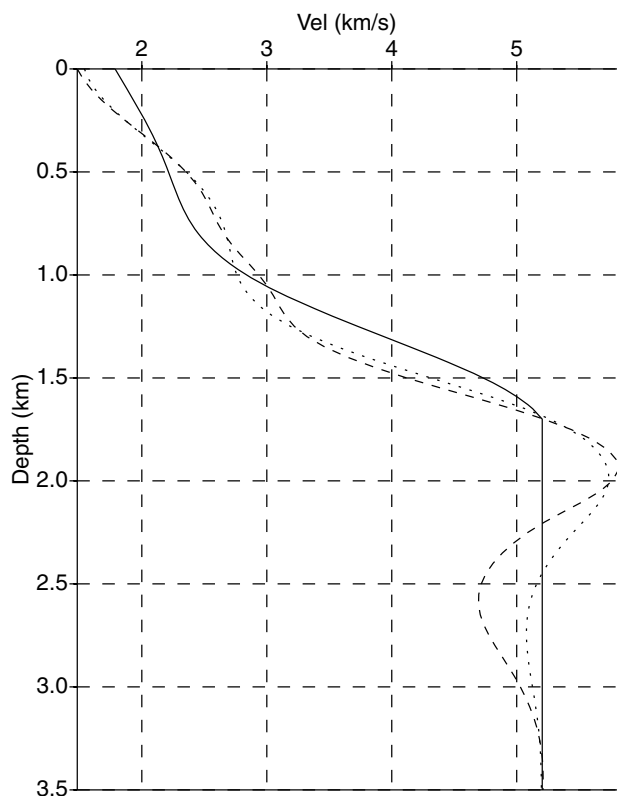


**Figure 9** Real data case. Velocities profile comparison at the position  $X = 9$  km. Solid line: initial velocity model, dashed line: depth picking, dotted line: time picking.

While the stretching factor,  $q_z^{ray}$ , can be obtained using a migration of attributes, the residual slope,  $\varphi$ , has to be picked somehow on the common-image gathers. Stereotomographic picking involves slope picking on prestack un-migrated data. A similar process to the one used in standard stereotomographic picking (Billette *et al.* 2003), may be applied for the picking of  $\varphi$  (Chauris *et al.* 2002a,b).

Finally, starting from a prestack depth migrated cube, we see that through the picking of the residual slope in common-image gathers and migration of attributes for  $s$ ,  $r$ ,  $T^{ray}$ ,  $p_s^{ray}$ ,  $p_r^{ray}$ , and  $q_z^{ray}$ , we can build a stereotomographic dataset theoretically whatever the quality of the velocity model used for the initial depth migration.

### Stereotomography with picking in depth

The workflow we propose for depth velocity model building involves a full sequence of processes. First, we have the determination of the stereotomographic dataset from an initial pre-stack depth migration. Then, from this stereotomographic

dataset, a stereotomographic optimization updates the depth velocity model.

For the determination of the stereotomographic dataset, we propose the following workflow:

- 1 Migration of depth domain attributes ( $T^{ray}$ ,  $s^{ray}$ ,  $r^{ray}$ ,  $p_s^{ray}$ ,  $p_r^{ray}$ ,  $q_z^{ray}$ ). We use a 2.5D Kirchhoff common-offset preserved amplitude migration code (Nguyen *et al.* 2002a) adapted for migration of attributes. It is based on wavefront construction (Lambaré, Lucio and Hanyga 1996) which allows us to obtain all the necessary attributes.

- 2 For the selected common-image gathers located at position  $x^{mig}$  and around offset,  $h^{mig}$ , we perform an automated picking of the depth,  $z^{mig}$  and residual slope,  $\tan(\varphi)$  of the local events. The automated picking is based on local slant stack panels and is directly adapted from the automated picking tool presented in Lambaré *et al.* (2004).

- 3 At the location of the picked events ( $x^{mig}$ ,  $z^{mig}$ ,  $h^{mig}$ ), we perform an extraction of the attributes using relation (9). Some regularization is introduced (Baina *et al.* 2002) in order to avoid instabilities. From these attributes we directly obtain stereotomographic parameters, ( $s^{data}$ ,  $r^{data}$ ,  $T^{data}$ ).

- 4 We finally use the value of the residual slope,  $\tan(\varphi)$ , picked on the common-image gathers at locations ( $x^{mig}$ ,  $z^{mig}$ ,  $h^{mig}$ ), in combination with attributes ( $p_{sx}^{ray}$ ,  $p_{rx}^{ray}$ ,  $q_z^{ray}$ ), and apply the *imaging equations* (relations (11) and (12)). We obtain the stereotomographic slopes ( $p_s^{data}$ ,  $p_r^{data}$ ).

For the stereotomographic optimization we use the algorithm described in Billette *et al.* (2003) or Lambaré *et al.* (2004). Stereotomography is a slope tomography method by which the velocity model is optimized jointly with the pairs of ray segments. The misfit function involves all the picked parameters (see expression (10)). In practice, rays are shot from the reflecting/diffracting point towards the source and receiver positions, for two given starting angles and two one-way travel times.

The algorithm of stereotomography can be decomposed into three steps:

- 1 initialisation of velocity model and of the pairs of ray segments;
- 2 relocalisation of the ray segments in the initial velocity model using a non linear quasi-Newton optimization scheme;
- 3 joint optimization of ray segments and velocity model using a non linear least-square-root scheme Paige and Saunders (1982).

We consider smooth velocity models described by cubic cardinal B-splines, which are direct inputs for the ray based migration/inversion. Some regularization is introduced in order to stabilize the optimization (Alerini *et al.* 2007).

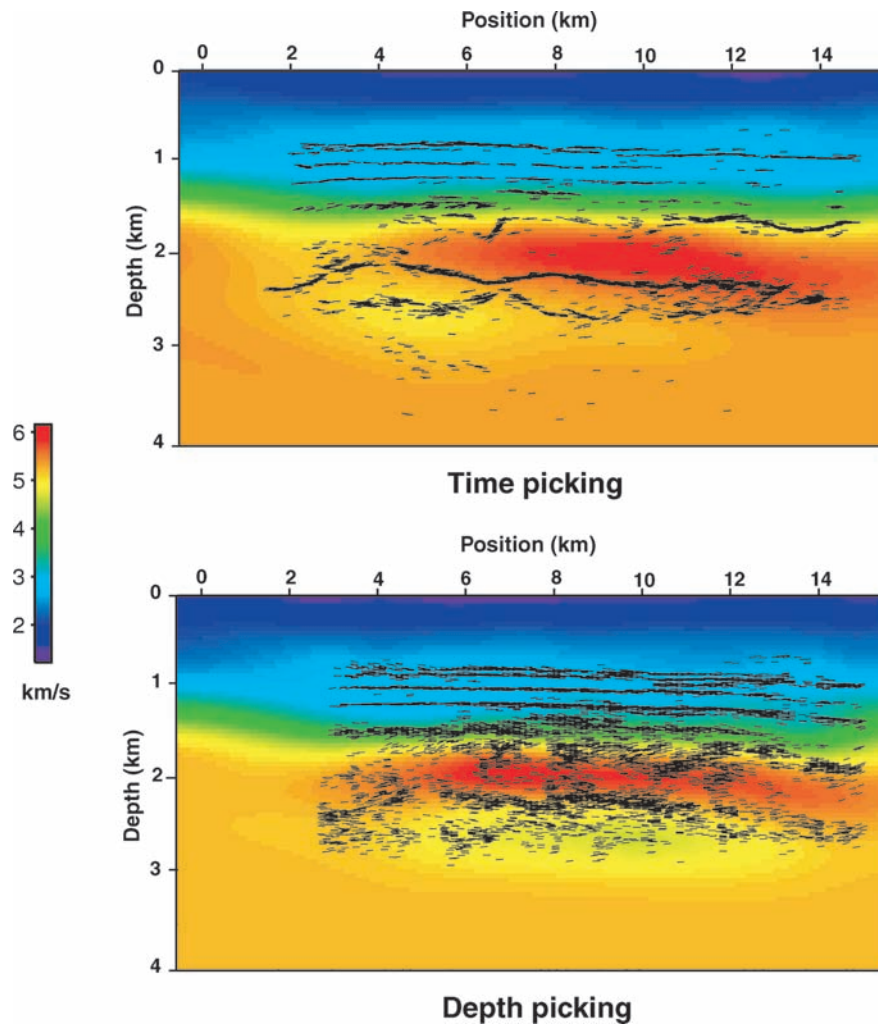


**Figure 10** Real data case. Inverted velocity models with the dipbars (location and dip of inverted local events) superimposed. Top: results for 3900 events picked in the time un-migrated domain. Bottom: results for 7800 events picked in the depth migrated domain.

## APPLICATIONS

### Synthetic data validation of the stereotomographic picking

We created a 2D synthetic model where four curved reflectors are superimposed onto a smooth background with a constant gradient of velocity with a tilted axis (Fig. 3). We generated a 2D seismic data using a Kirchhoff modelling algorithm (Baina *et al.* 2002).

With this dataset, we had the opportunity to test our stereotomographic picking in depth. In particular, we wanted to test its sensitivity to the velocity model used for the initial pre-stack depth migration. Let us do depth migration using as velocity model the one resulting from the overall multiplication of the exact velocity model by a factor of 1.1 (10% perturbation). Only three attributes are considered here, namely

time, receiver location and source slope. The others exhibit similar behaviour. We consider a single reflector, the third one from the top and a single offset (offset = 100 m). Figure 4 shows the corresponding common offset depth migrated image. We see that the migrated interface is not at the correct depth.

Figures 5, 6 and 7 present comparisons of migrated attributes, two way time, receiver location and source slope, respectively. For the source slope we show the results with and without the residual slope corrections (respectively green and blue curves). We compare all these results picked in the depth migrated domain to the values picked in the time un-migrated domain (red curve). As expected, we can see that the picked surface locations and traveltimes are immediately valid from the migration of attributes, while the migrated slopes,  $p_s^{ray}$ ,

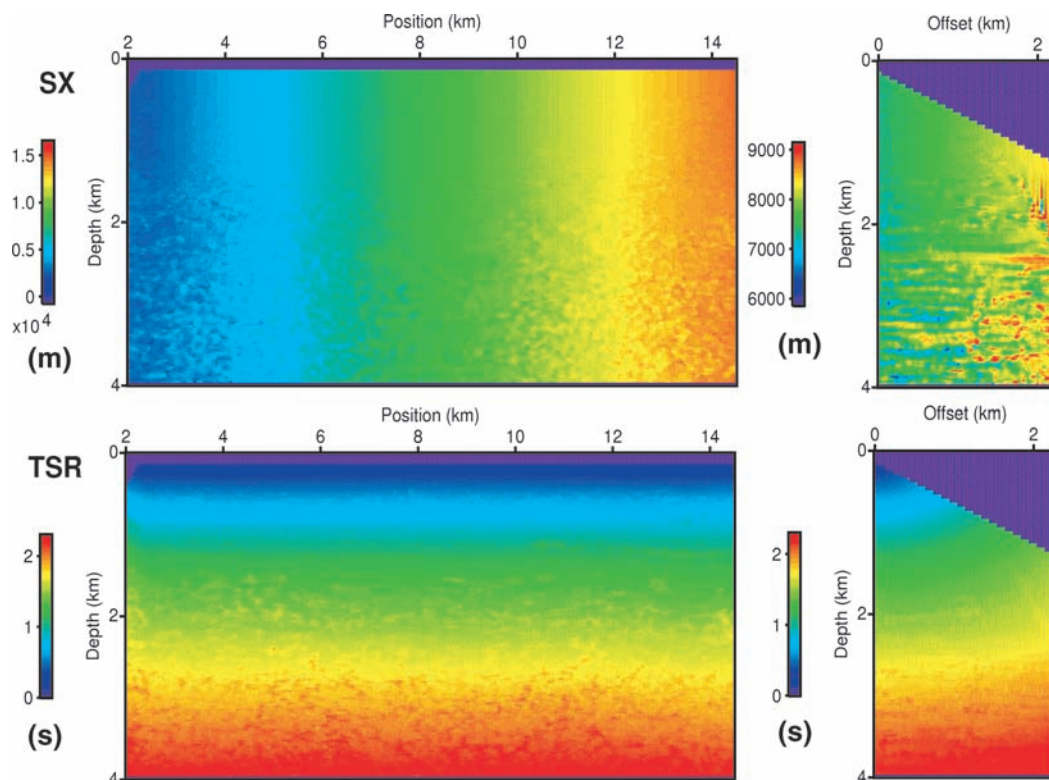


**Figure 11** Real data case. Inverted attribute map: Left) common offset profile, for offset = 100 m; Right) common-image gather, for  $x = 9$  km: Top) source location,  $s^{ray}$ ; Bottom) two-way traveltime,  $T^{ray}$ .

are correct only when applying the residual slope corrections (relations (12) and (13)).

Note that the picking of slopes done in the time un-migrated domain exhibits some artefacts (Fig. 7) because of the triplicated reflection (Fig. 3). In depth, even if the wrong velocity macro-model was used for migration (Fig. 4), the triplication is unfolded and leads to an easier slope picking without artefacts (Fig. 7). Note that there is no general statement about the unfolding of the triplications when performing depth migration with the wrong velocity model but it certainly improves when the velocity model is not too far from the exact one.

## Real data application

### Data

The 2D marine pre-stack data was extracted from a 3D data set using a cross-line isotropic time migration (Devaux, Gardner and Rampersad 1996). An attenuation of multiples was applied. There are 1011 shot points with an offset range from 112.5 m to 2387.5 m, a shot interval of 12.5 m and a receiver spacing of 25 m. The time sampling is 4 ms. Figure

8 shows the 500 m common offset section. Note that the section exhibits a good signal-to-noise ratio, which is favourable to stereotomographic picking in the time domain. There is a strong vertical velocity contrast due to a salt body. The dataset was used for several other applications of slope tomographic methods (Le Bégat, Podvin and Lambaré 2000; Chauris *et al.* 2002b). In all these applications there was a systematic shift in depth (the migrated interfaces appear too deep when compared to the well information) that could only be tackled with anisotropic tomography (Devaux 2000). In our application, we will definitely stay within isotropic approximation but we investigate whether some improvement in the stereotomographic picking could lead to a better well matching.

### Picking and inversion

The initial velocity field for our inversion test is a 1D model (Fig. 9). To validate our method, we performed two 2D velocity model inversions: the first one with events picked in the time un-migrated domain, the second with events picked in the depth migrated domain according to the procedure we propose. The automated picking tool for locally coherent events,

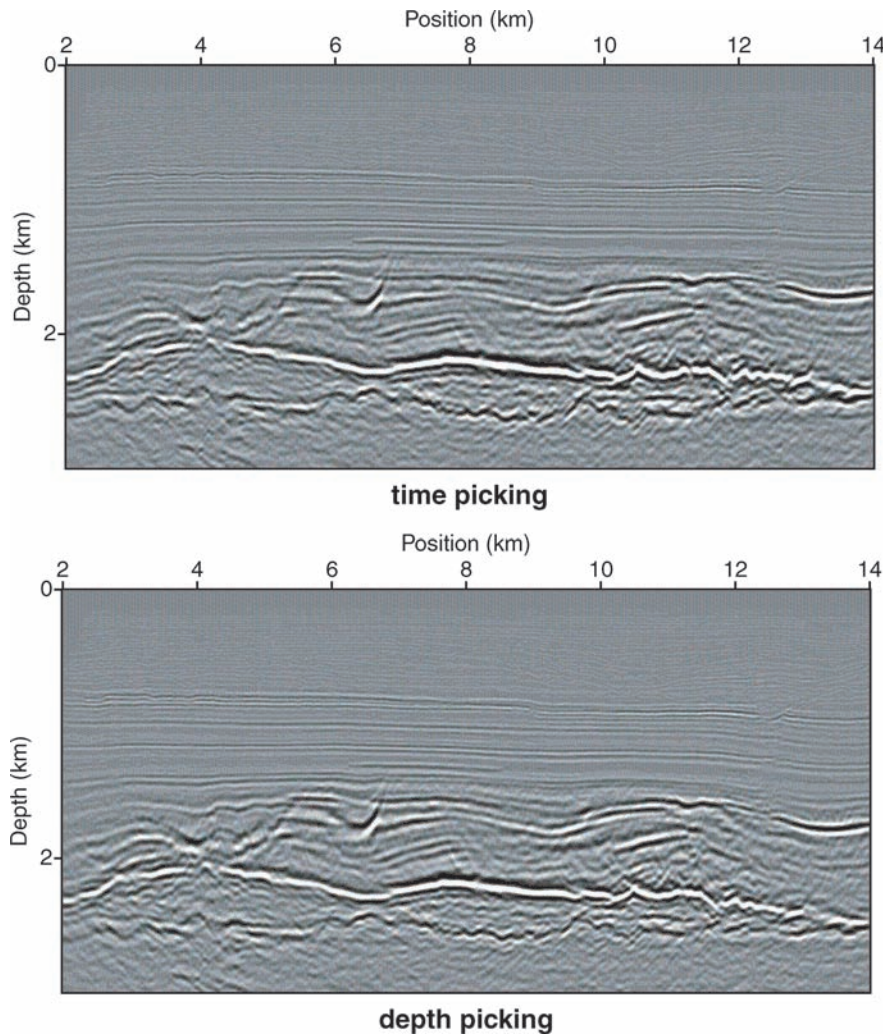


**Figure 12** Real data case. Migrated image obtained using the inverted velocity models obtained from the stereotomographic time picking (top) and the depth picking (bottom).

both in time and depth, is based on local slant stack panels (the same tool was used for the synthetic data validation (Billette *et al.* 2003; Lambaré *et al.* 2004)).

For the picking in the time un-migrated domain we picked each 50 m in shot position and each 200 m in receiver position for an offset range of [388, 2188] m. 3900 reliable picks could be successfully inverted after 100 non-linear iterations of the joint optimization. In order to keep a reasonable ratio between data and unknowns, the velocity model is described by B-spline nodes with 500 m horizontal and 125 m vertical spacing. Figure 10 (top) shows the inverted velocity macro-model, superimposed with the dipbars (location and dip of inverted local events) corresponding to the time picking mapped in depth. Only the main reflectors were detected by the auto-

mated picking tool, leading to a poor coverage of the velocity model in depth. Relaxing of the automated picking criteria allowed us to densify the picking in depth but then the number of inconsistent picked events prevented our stereotomographic optimization from converging.

For the picking in the depth migrated domain, we used the pre-stack depth migrated cube obtained using the 1D initial velocity model (Fig. 9). Figure 11 shows the migration of attributes for attributes  $s^{ray}$ , and  $T^{ray}$ . We picked each 125 m in position, and each 125 m in offset for an offset range of [325, 2362] m. The first 4000 picks were inverted for about 50 non-linear iterations of the joint optimization. However, the better signal-to-noise ratio in the depth migrated domain allowed us to invert a denser picking (7800 events). Using

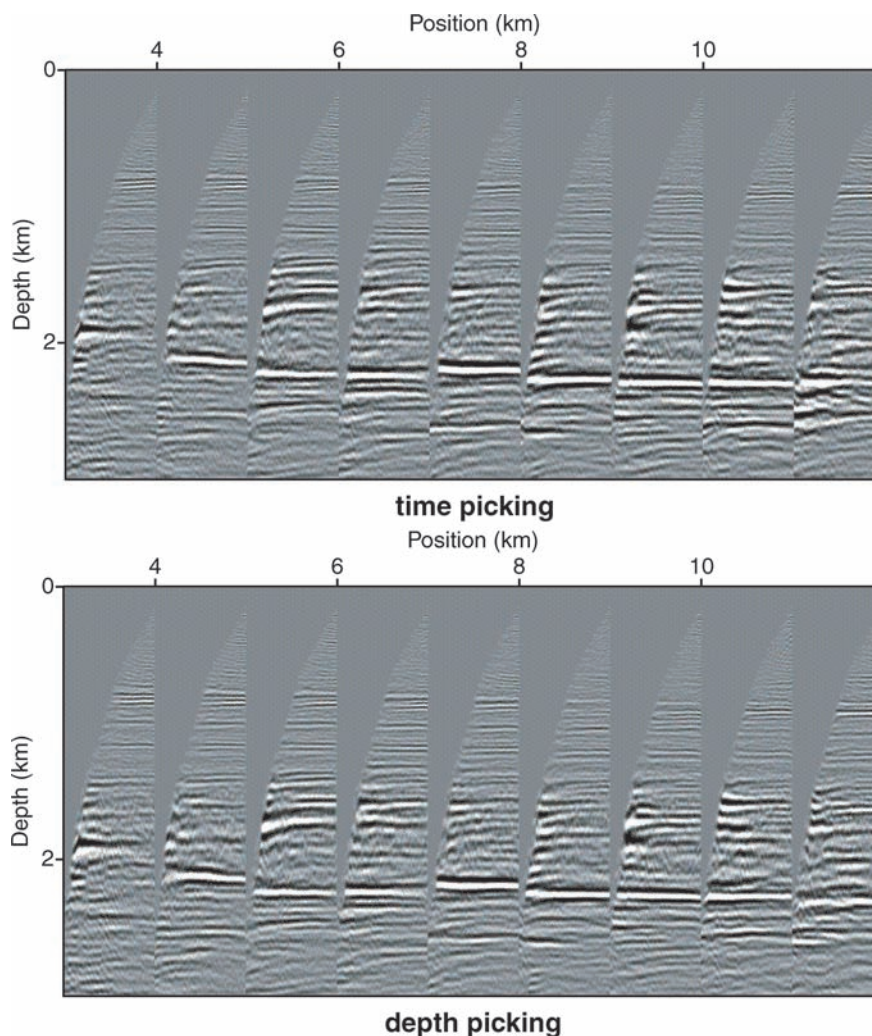


**Figure 13** Real data case. Common-image gathers obtained using the inverted velocity models obtained from the stereotomographic time picking (top) and the depth picking (bottom). The offset range is from 112.5 m to 2387.5 m.

this new dataset we first performed 20 non-linear iterations of the joint optimization. Figure 10 (bottom) shows the dense depth picking and the associated inverted velocity model. We see that the depth picking covers the main interfaces as well as above and inside the salt body ( $z = 2$  km to  $z = 2.8$  km). This improved spatial distribution of the picking explains the improved recovery of the vertical velocity contrasts as shown in Fig. 9. The velocity anomaly, due to the presence of salt (around  $z = 2$  km), is definitely clearer when using the depth picking.

#### *Depth migrated images*

Let us have a look now at the depth migrated images obtained with a preserved-amplitude Kirchhoff algorithm (Nguyen

*et al.* 2002a). The migration stacks appear quite similar for the results obtained with the depth and time picking (Fig. 12), nevertheless some slight improvements in the focusing can be observed in the final migrated image (Fig. 14) obtained with depth picking (same gain was applied to the migrated images). Moreover, the common-image gathers are quite well flattened (Fig. 13).

Note that for the depth picking result, due to the large amount of data, the B-spline grid could be densified to  $\Delta X = 250$  m and  $\Delta Z = 75$  m. Additional inversion loops (50 iterations) gave an improvement for the depth position of reflectors. We compare in Fig. 15 our results with some reflector depths obtained from a well (Devaux 2000). For the coarse B-splines parameterization, similar depths (Figs 15a and b) are obtained with time and depth picking velocity models. For

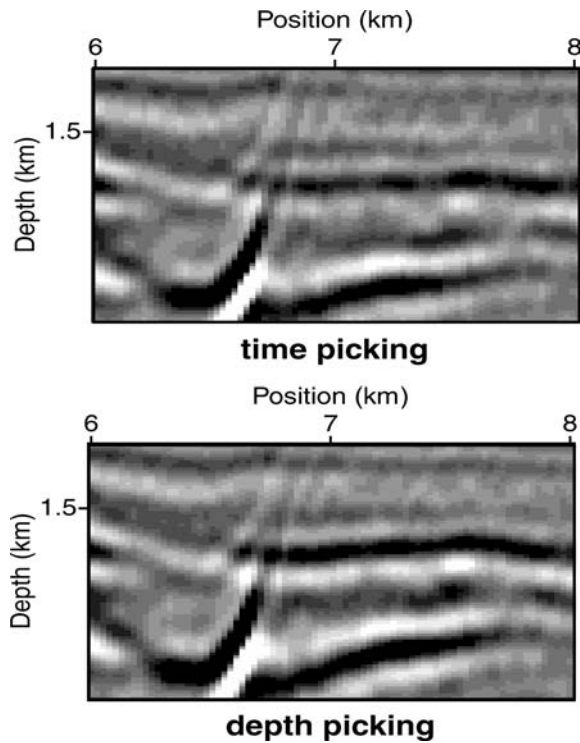


**Figure 14** Real data case. Zoom on migrated images obtained using the inverted velocity models obtained from the stereotomographic time picking (top) and the depth picking (bottom). The depth migrated image obtained with the depth picking exhibits higher amplitude, demonstrating the better focusing when compared to the depth migrated image obtained with the time picking.

the denser B-splines parameterization, we obtain an improved positioning of the deepest reflectors with the depth picking velocity model (Fig. 15c).

#### Analysis of residuals

The cost function of Stereotomography involves misfits for all parameters of data,  $d$ , (expression (10)). Figure 16 shows the iterative minimization of the square root of the cost function (normalized according to the number of events). For the curve associated with the optimization of the depth picking datasets, we can clearly identify the three steps of the optimization. First, the inversion for the first dataset with 4000 events, then the inversion for the denser dataset with 7000 events, and finally, for the densification of the B-spline grid with 7000 events. Note that there is an increase of the normalized cost function each time we change the dataset or the velocity grid. This is due to the fact that each time we restart the stereotomographic optimization process without taking advantage of the information gained on the pairs of ray segments or on the velocity model in the previous results. Nevertheless, we

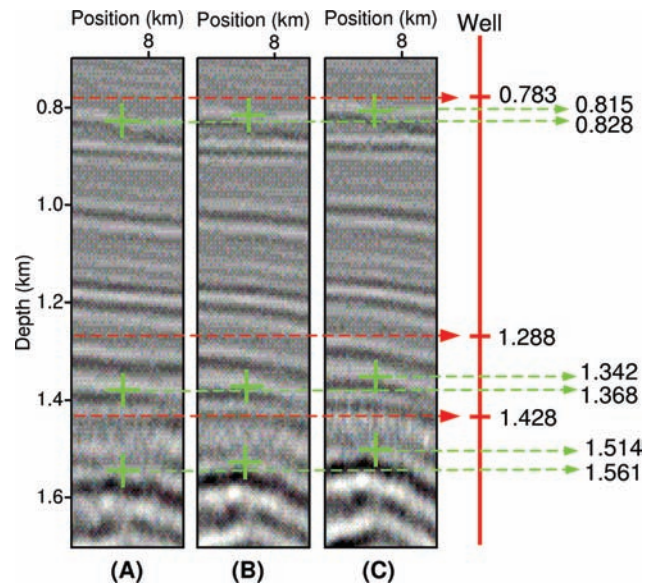


**Figure 15** Real data case. Comparison of the migrated images obtained for various inverted velocity models with some depth interpreted from a well: (a) Stereotomography with time picking (3900 events) and B-splines sampling  $\Delta X = 500$  m,  $\Delta Z = 125$  m. (b) Stereotomography with a dense depth picking (7800 events) and B-splines sampling  $\Delta X = 500$  m,  $\Delta Z = 125$  m. (c) Stereotomography with a dense depth picking (7800 events) and B-splines sampling  $\Delta X = 250$  m,  $\Delta Z = 75$  m. The depth of three selected horizons in the well are indicated on the right and reported on the migrated images with dashed red lines. The depth of the corresponding horizons picked in the migrated images are indicated by green crosses and reported on the well with green dashed lines.

see that the three curves are converging and provide a better normalized misfit than for the time picking (Fig. 16).

## CONCLUSIONS

We have shown with this study that stereotomography was not limited to picking in the time unmigrated domain. We have proposed a robust and efficient strategy for picking stereotomographic attributes in the depth migrated domain. No kinematic demigration is used as in Chauris *et al.* (2002a) but we use migration of attributes for getting source and receiver positions, time and various components of slowness vectors. The residual slope of the events is then picked on common-image gathers and, in combination with the components of slowness vectors obtained by migration of attributes, it is used to derive the slopes of the event in the unmigrated time domain. This correction ensures that the stereotomographic dataset is valid, even if the velocity model used for the depth migration is erroneous.

If both time unmigrated data and the depth migrated data are available for stereotomographic picking, the preferable

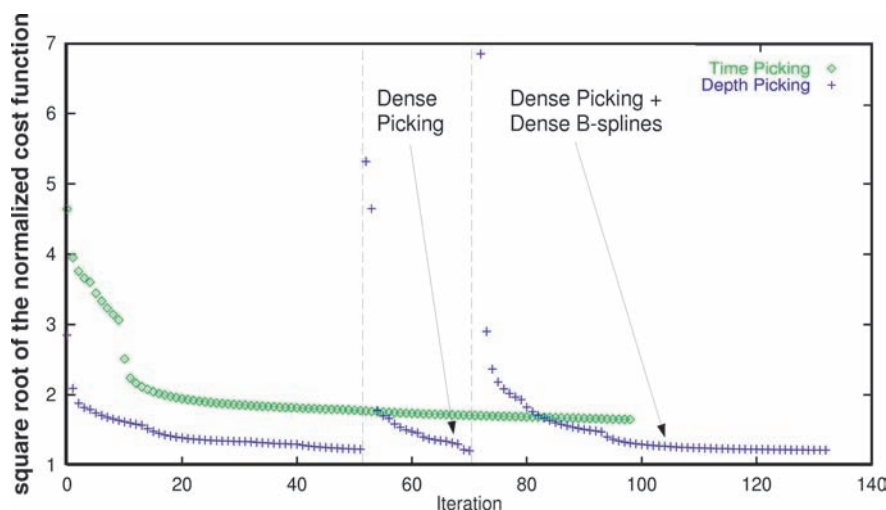


Figure 16 Real data case. Variation of the cost function during the iterative minimization. The cost function is normalized according to the number of picked events.

domain will be the one exhibiting the higher signal-to-noise ratio with the minimum overlapping of locally coherent events. Depth migration domain may frequently qualify even when an erroneous velocity model is used. However, when no initial depth migrated result is available and when the quality of the un-migrated dataset is appropriate, the stereotomographic picking can still be advantageously performed in the time un-migrated domain.

Finally, we validated our new depth picking approach on synthetic data, and then we applied the full stereotomographic workflow to a real dataset. We compared the results of a stereotomographic time picking and depth picking process and demonstrated that due to a better coverage of the velocity model, the depth picking provided a slightly improved result. It is clear that for cases where depth migrated results exhibit a much higher signal-to-noise ratio than the un-migrated traces, the advantage of using stereotomographic picking in the depth migrated domain would be more significant.

## ACKNOWLEDGEMENTS

The authors thank the sponsors of DIG consortium. This work has been partly supported by the French 'Fonds de Soutien aux Hydrocarbures' (Ministry of Industry).

The authors also thank Pascal Podvin for providing the slope picking tool, Soazig Le Béat and Philippe Thierry for fruitful discussions.

They are grateful to Total (formerly TotalFinaElf) for providing the real data and for permission to present the results.

## REFERENCES

- Alerini M., Le Béat S., Lambaré G. and Baina R. 2002. 2D PP- and PS-stereotomography for a multicomponent dataset. 72nd SEG meeting, Salt Lake City, Utah, USA, Extended Abstracts, 838–841.
- Alerini M., Lambaré G., Baina R., Podvin P. and Le Béat S. 2007. Two-dimensional PP/PS-Stereotomography: P- and S-waves velocities estimation from OBC data. *Geophysical Journal International* 170, 725–736.
- Al-Yahya K. 1989. Velocity analysis by iterative profile migration. *Geophysics* 54, 718–729.
- Apostoiu-Marin I. and Ehinger A. 1997. Kinematic interpretation in the prestack depth-migrated domain. *Geophysics* 62, 1226–1237.
- Baina R., Thierry P. and Calandra H. 2002. Demonstration of 3D preserved amplitude PSDM & AVA relevance. *The Leading Edge* 21, 1237–1241.
- Bender C. and Orszag S. 1978. *Advanced Mathematical Methods for Scientists and Engineers*. McGraw-Hill, New York.
- Billette F. and Lambaré G. 1998. Velocity macro-model estimation from seismic reflection data by stereotomography. *Geophysical Journal International* 135, 671–680.
- Billette F., Le Béat S., Podvin P. and Lambaré G. 2003. Practical aspects and applications of 2D stereotomography. *Geophysics* 68, 1008–1021.
- Bleistein N. and Handelsman R. 1975. *Asymptotic Expansions of Integrals*. Dover Publications Inc.
- Bleistein N. 1987. On the imaging of reflectors in the Earth. *Geophysics* 52, 931–942.
- Chalard E. and Lambaré G. 2005. Status of 3D stereotomographic optimization. 75th SEG meeting, Houston, Texas, USA, Extended Abstracts, TOM P1.2.
- Chalard E., Podvin P., Lambaré G. and Audebert F. 2000. Principles of 3-D Stereotomography. 62nd EAGE meeting, Glasgow, UK, Extended Abstracts, P-144.

- Chauris H. and Noble M. 2001. 2D velocity macro model estimation from seismic reflection data by local Differential Semblance Optimization; applications on synthetic and real data. *Geophysical Journal International* **144**, 14–26.
- Chauris H., Noble M., Xu S. and Lambaré G. 2001. Migration velocity analysis in complex media: application to the Marmousi data set. 63rd EAGE meeting, Amsterdam, The Netherlands, Extended Abstracts, M–33.
- Chauris H., Noble M.S., Lambaré G. and Podvin P. 2002a. Migration velocity analysis from locally coherent events in 2-D laterally heterogeneous media, Part I: Theoretical aspects. *Geophysics* **67**, 1202–1212.
- Chauris H., Noble M.S., Lambaré G. and Podvin P. 2002b. Migration velocity analysis from locally coherent events in 2-D laterally heterogeneous media, Part II: Applications on synthetic and real data. *Geophysics* **67**, 1213–1224.
- Chauris H. 2000. *Analyse de vitesse par migration pour l'imagerie des structures complexes en sismique réflexion*. PhD thesis, École des Mines de Paris.
- Chen J. 2000. Specular-ray parameter extraction and stationary-phase migration. 70<sup>th</sup> SEG meeting, Calgary, Canada, Expanded Abstracts, 794–797.
- Devaux V., Gardner G.H.F. and Rampersad T. 1996. 3D prestack depth migration by Kirchhoff operator splitting. 66th SEG meeting, Denver, Colorado, USA, Expanded Abstracts, 455–458.
- Devaux V. 2000. Anisotropic 2.75-D PsDM Imaging: a first application to 3-D field data. 62<sup>nd</sup> EAGE meeting, Glasgow, UK, Workshop W2.
- Farra V. and Madariaga R. 1988. Non-linear reflection tomography. *Geophysical Journal* **95**, 135–147.
- Gosselet A., Le Bégat S. and Petersen S. 2005. Joint slope tomography of borehole transmitted and surface seismic data. 75th SEG meeting, Houston, Texas, USA, Extended Abstracts, TOM 2.5.
- Hubral P., Schlecher J. and Tygel M. 1996. A unified approach to 3-D seismic reflection imaging, part I: Basic concepts. *Geophysics* **61**, 742–758.
- Jäger R., Mann J., Höcht G. and Hubral P. 2001. Common-reflection-surface stack: image and attributes. *Geophysics* **66**, 97–109.
- Lambaré G., Lucio P.S. and Hanyga A. 1996. Two-dimensional multi-valued traveltimes and amplitude maps by uniform sampling of ray field. *Geophysical Journal International* **125**, 584–598.
- Lambaré G., Alerini M., Baina R. and Podvin P. 2004. Stereotomography: a semi-automatic approach for velocity macro-model estimation. *Geophysical Prospecting* **52**, 671–681.
- Lavaud B., Baina R. and Landa E. 2004. Automatic robust velocity estimation by poststack stereotomography. 74<sup>th</sup> SEG meeting, Denver, Colorado, USA, Extended Abstracts, 3251–3254.
- Le Bégat S., Podvin P. and Lambaré G. 2000. Stereotomography: strategy for application to real data in 2D. 62nd EAGE meeting, Glasgow, UK, Extended Abstracts, L–46.
- Le Stunff Y. and Grenier D. 1998. Taking into account a priori information in 3D tomography. 68<sup>th</sup> SEG meeting, New Orleans, Louisiana, USA, Expanded Abstracts, 1875–1878.
- Liu Z. 1997. An analytical approach to migration velocity analysis. *Geophysics* **62**, 1238–1249.
- Neckludov D., Baina R. and Landa E. 2005. Residual stereotomographic inversion. *Geophysics* **71**, E35–E39.
- Nguyen S., Baina R., Noble M. and Thierry P. 2002a. Ray-based anti-aliasing for depth migration. 64th EAGE meeting, Florence, Italy, Extended Abstracts, A–36.
- Nguyen S., Baina R., Noble M. and Thierry P. 2002b. Tomography picking in the depth migrated domain using migration of attributes. 72nd SEG meeting, Salt Lake City, Utah, USA, Expanded Abstracts, 1140–1143.
- Paige C. and Saunders M.A. 1982. LSQR: An algorithm for sparse linear equations and least squares. *ACM Transactions on Mathematical Software* **8**, 43–71.
- Riabinkin L.A. 1957. Fundamentals of resolving power of controlled directional reception (CDR) of seismic waves. In: *Slant Stack Processing*, pp. 36–60. Geophysics reprint series, Volume 14, 1991 SEG. (Translated and paraphrased from *Prikladnaya*, 16, 3–36).
- Sword C.H. 1986. Tomographic determination of interval velocities from picked reflection seismic data. 56<sup>th</sup> SEG meeting, Houston, Texas, USA, Expanded Abstracts, 657–660.
- Symes W.W. 1998. High frequency asymptotics, differential semblance, and velocity estimation. 68th SEG meeting, New Orleans, Louisiana, USA, Expanded Abstracts, 1616–1619.
- Thierry P., Lambaré G., Podvin P. and Noble M. 1999. 3-D preserved amplitude prestack depth migration on a workstation. *Geophysics* **64**, 222–229.
- Tygel M., Schleicher J. and Hubral P. 1994. Pulse distortion in depth migration. *Geophysics* **59**, 1561–1569.
- Tygel M., Schleicher J. and Hubral P. 1996. A unified approach to 3-D seismic reflection imaging, part II: Theory. *Geophysics* **61**, 759–775.
- Wang Y. and Houseman G.A. 1995. Tomographic inversion of reflection seismic amplitude data for velocity variation. *Geophysical Journal International* **123**, 355–372.
- Wang Y., White R. and Pratt G. 2000. Seismic amplitude inversion for interface geometry: practical approach for application. *Geophysical Journal International* **142**, 162–172.